

26 May 2010, 4:45 pm - 6:45 pm

# Residual Strength of Liquefied Sand: Laboratory vs. Field Measurements

Julián Sandoval
*University of New Hampshire, Durham, NH*

Pedro de Alba
*University of New Hampshire, Durham, NH*

Thomas P. Ballestero
*University of New Hampshire, Durham, NH*

Barry K. Fussell
*University of New Hampshire, Durham, NH*


Fifth International Conference on
Recent Advances in Geotechnical Earthquake Engineering and Soil Dynamics
*and Symposium in Honor of Professor I.M. Idriss*
May 24-29, 2010 • San Diego, California

# RESIDUAL STRENGTH OF LIQUEFIED SAND: LABORATORY VS. FIELD MEASUREMENTS

**Julián Sandoval**
University of New Hampshire
Durham, NH 03824

**Pedro de Alba**
University of New Hampshire
Durham, NH 03824

**Thomas P. Ballestero**
University of New Hampshire
Durham, NH 03824

**Barry K. Fussell**
University of New Hampshire
Durham, NH 03824

ABSTRACT

Determining the residual strength of liquefied sand is essential for estimating post-earthquake stability of vulnerable earth structures, or calculating runout of liquefaction flow slides. Current practice is to select values from a database of back-calculated residual strengths from failure case histories , which have been related to representative penetration test resistance numbers in the failed materials. Given the uncertainties involved, it is desirable to compare the field data with laboratory tests under controlled conditions. This paper describes residual strength measurements for a uniform fine sand using two recently-developed tests designed to impose large strains and strain rates: a modified triaxial test in which a metal coupon is dragged through the liquefied sample by an external dead weight, and a ring shear device which can impose constant rates of strain on the liquefied sand. In all cases, a stress-thinning behavior is observed; however, coupon movement through the liquefied sand is basically laminar, representing conditions in the interior of a flowing mass, while the rotating ring creates a well-defined contact shear band and higher resistance, which might be considered more representative of flow at the base of a sliding mass. Comparison with back-calculated field values shows that coupon residual strengths plot at the lower bound, and ring shear results at the upper bound, of back-calculated field values.

## INTRODUCTION

Earthquake-induced liquefaction flow slides are of major concern in both natural slopes and earth structures. Determining potential runout, or deciding on remedial measures, requires modeling the behavior of the liquefied material. Current practice is to select a single representative value of residual strength (Sur) for this purpose, relying basically on Sur -values back-calculated from collections of case histories of liquefaction failures, as originally proposed by H. B. Seed (1986). These collections have been re-examined and expanded by other researchers, (e.g. Seed and Harder, 1990, Olson and Stark, 2002, Idriss and Boulanger, 2007).

In this approach, Sur-values are related to representative values of field penetration resistance, obtained either from the cone penetrometer or, predominantly, from the standard penetration test (SPT). Given the difficulties of deciding on a single representative value of Sur from the complex post-failure geometry of a failed slope and the available penetrometer data, it is not surprising that there is a considerable scatter in these values.

Consequently, in order to produce improved models of liquefied soils, laboratory tests under controlled conditions would be very helpful; however, conventional geotechnical laboratory tests cannot reproduce the strain levels and strain rates occurring in the sliding material. Described below are results obtained using two different devices that were designed specifically to produce high strain levels and strain rates in the same liquefied sand.

## COUPON TESTS

In order to study the evolution of Sur at high velocities and strain levels, series of stress-controlled experiments were carried out, in which a smooth square coupon was embedded in a long triaxial specimen, which was liquefied by cyclic loading. The behavior of the coupon was observed as it was drawn lengthwise through the liquefied soil by a deadweight system. The hydrodynamic behavior of the coupon was

analyzed modeling the liquefied soil as a viscous fluid (de Alba and Ballestero, 2005). Figure 1 is a schematic of the experimental device; tests were carried out by forming triaxial specimens of sand around a 2.54-cm smooth square titanium coupon, 0.16 cm thick, attached to a fine (0.081 cm-diameter) wire which could slide through an o-ring seal in the chamber base.

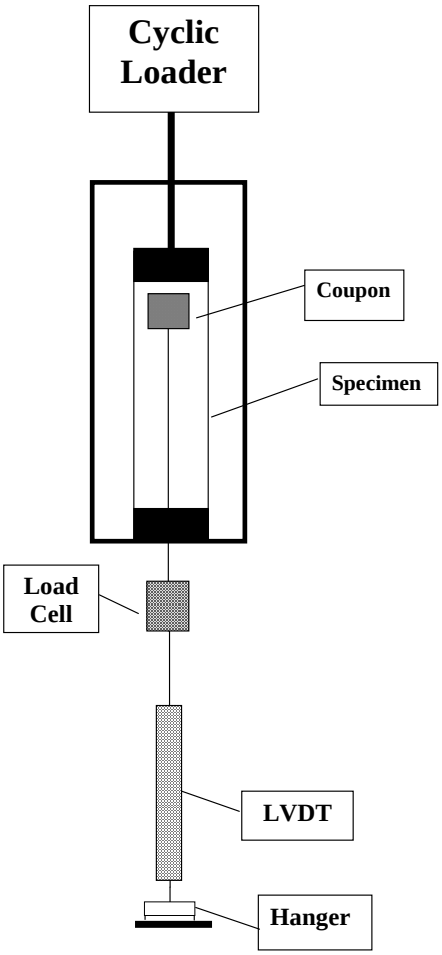


*Fig. 1. Schematic of Triaxial coupon test (not to scale)*

Triaxial specimens were approximately 24 cm (9.5 in) high and 7.1 cm (2.8 in) in diameter. The coupon was placed in the specimen so that it could travel approximately 17.8 cm (7 in) before the weight hanger hit its support, thus stopping the coupon about 2.5 cm (1 in) above the base of the specimen. The coupon's displacement and resistance to motion were measured by a load cell and LVDT arrangement as shown in the figure.

A uniform fine quartz sand, "Holliston 00" (SP) with semi-angular grains was used for this study. Material properties are as follows, with reported maximum and minimum densities obtained by Japanese standard test method JIS A 1224. the fines content was less than 1%.

Mean grain diameter $D_{50}$= 0.3 mm

Coefficient of uniformity Cu =1.9

Coefficient of curvature Cc = 1.6

Max. dry density, $\gamma_d$ max = 16.2 kN/m$^3$

Min. dry density $\gamma_d$ min = 13.4 kN/m$^3$

Specimens were formed by a modified pluviation method, as follows:

1. A mold/membrane stretcher was assembled around the specimen base; the coupon on its wire was positioned at 20.3 cm above the base.

2. The mold was filled with dry sand, and a 20-cm long capped sleeve was attached to the top of the mold. The mold and sleeve assembly was then slowly rotated vertically several times to re-deposit the sand. During rotation, the coupon was held in position by a fine thread extending through the cap on the sleeve.

3. The triaxial chamber was then assembled around the specimen, and it was saturated by circulating $CO_2$ followed by de-aired water, and then applying a back pressure of 70 kPa. Skempton B-values of 0.95 or higher were obtained for all tests discussed here.

The triaxial system was set up to stop cycling when axial strains exceeded $\pm$ 2 %, typically one cycle after initial liquefaction (pore pressure ratio, $r_u = \Delta u/\sigma'_{vo}$ = 100%). Downward movement of the coupon was observed to start at initial liquefaction, and to continue after cyclic loading had stopped, until the weight hanger hit its base. Coupon drag and displacement values were taken 250 times/second.

Details of the original smooth coupon tests are reported in de Alba and Ballestero (2005). A subsequent series of tests, first reported here, was carried out to investigate the effect of coupon roughness by gluing a layer of the test sand to the surface of the coupon.

In order to obtain the shear stress exerted against the coupon, and the viscosity of the equivalent fluid, it was necessary to carry out a hydrodynamic analysis of the coupon movement, with emphasis on its behavior when it reached high strain rates and a 'stabilized' shear stress range.

Figure 2 compares the drag force measured by the load cell on the coupon as it was pulled through the liquefied sand, for smooth and rough coupons at approximately the same relative

density. All the tests described here were carried out starting from the same initial effective stress, $\sigma_o$'= 140 kPa (20 psi)

In order to obtain shear stress values and viscosities, the dynamic equilibrium of the coupon system for each time step had to be considered. A free body diagram of the coupon-wire system was drawn from above the coupon to just above the load cell (Fig. 1). From this free body diagram, a force balance equation in the vertical direction was prepared, in which the sum of the vertical forces was set equal to the mass of the coupon system in the free body diagram times its acceleration. Forces that acted included coupon weight buoyant force on the coupon, wire resistance, wire seal resistance, and the load cell reading (apparent drag). Since the wire length within the liquefied soil varied as the experiment progressed, the LVDT displacement measurements were used to compute the length of wire in the soil and thus the required correction for the buoyant force and shear resistance on the wire at any given time.

From the time histories of apparent (uncorrected) drag and coupon displacement (Fig. 2) the coupon velocity and acceleration were computed. The force balance analysis thus permitted the calculation of the corrected drag force on the coupon and, from the drag force, the shear stress on the faces

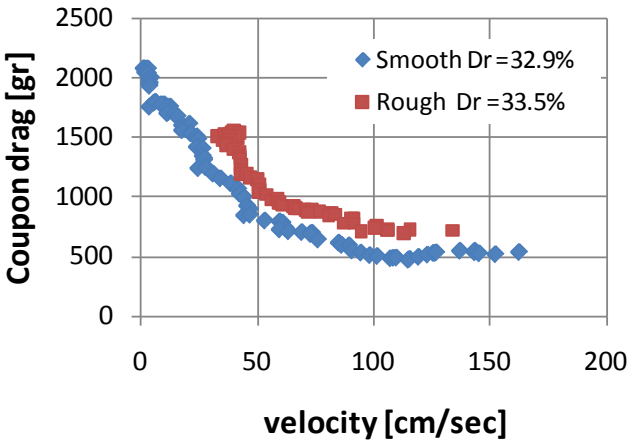


*Fig 2. Apparent (uncorrected) drag force on coupon vs. velocity, smooth and rough coupons*

of the coupon and the equivalent viscosity of the liquefied sand. Figure 3 compares equivalent viscosities of the rough and smooth coupons. In a 'well behaved' fluid the same viscosity might be expected, but in this case the equivalent viscosities of rough and smooth coupons varied by about half an order of magnitude, which may be attributed to a difference in shear band thickness on the face of the coupon. It is worth noting that for both smooth and rough coupons the Reynolds numbers were well below values for a turbulent boundary layer, thus indicating that a laminar flow model applied in both cases.

Different hanger weights were used in the test series, but these did not seem to have a significant effect on the 'stabilized drag' measured at large strains. Figure 4 shows the evolution of these drag values for a series of tests at approximately the same relative density, conducted with

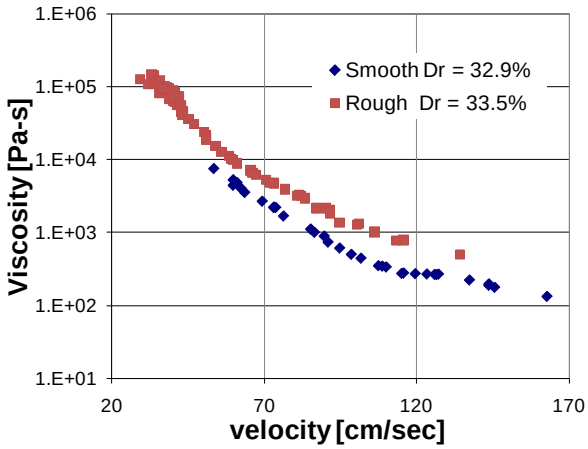


*Fig. 3. Equivalent fluid viscosity, smooth vs. rough coupon*

different hanger weights. These 'stabilized drag' values, obtained from the measured coupon drag as previously described, were used to calculate the large-strain, high-velocity shear stress (Sur) values shown in Fig. 5.

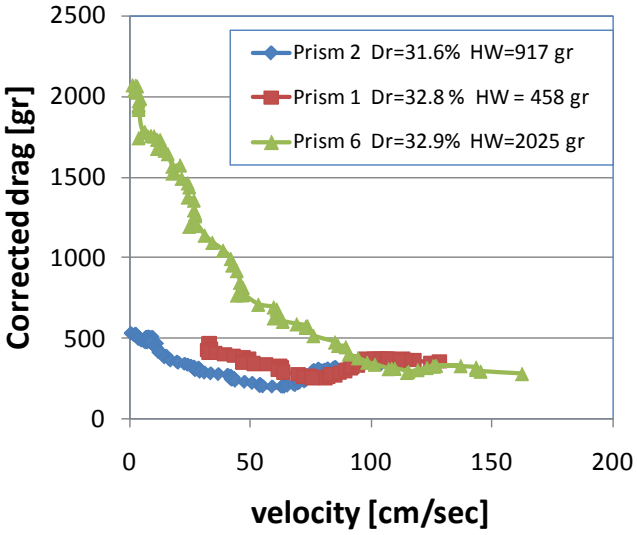


*Fig.4. Corrected coupon drag values for tests with different hanger weighs (HW) and similar realtive densities*

Figure 5 compares Sur results obtained from the rough and smooth coupons. In the Dr = 30-40% range tested for the rough coupons, the figure shows that, on the average, the stabilized Sur values for the rough coupons are about 35% higher than those for the smooth coupons. This may be attributed to differences in the behavior of the failure shear band forming around the coupons, as discussed below.

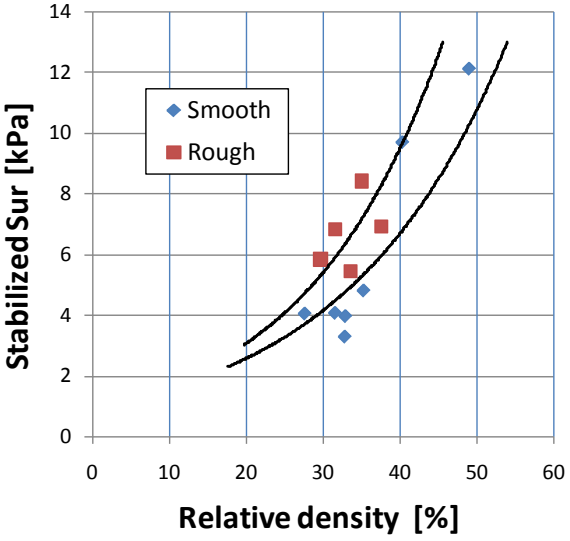


*Fig.5 Sur from large-strain stabilized coupon drag*

RING SHEAR TESTS

Results from the coupon tests suggested that the behavior of the liquefied sand was more complex than that which would be predicted from a simple Newtonian model and that it was best represented as a non-Newtonian stress-thinning fluid. Further study of this behavior required carrying out strain-controlled tests at speeds similar to those observed in the coupon tests. For this purpose, a relatively simple ring shear device was designed and built at UNH specifically for measuring the undrained residual strength of liquefied sand.

Figure 6 is a schematic of the device, which consists basically of two parts: (1) an annular soil container, and (2) a top ring and motor assembly which fits into the soil container, providing vertical confinement of the test specimen. The top ring can be rotated horizontally to produce cyclic or uni-directional horizontal shear stresses. The annular container and the top ring/motor assembly are mounted on moveable plates (lower plate and middle plate, Fig. 6). Alignment of the

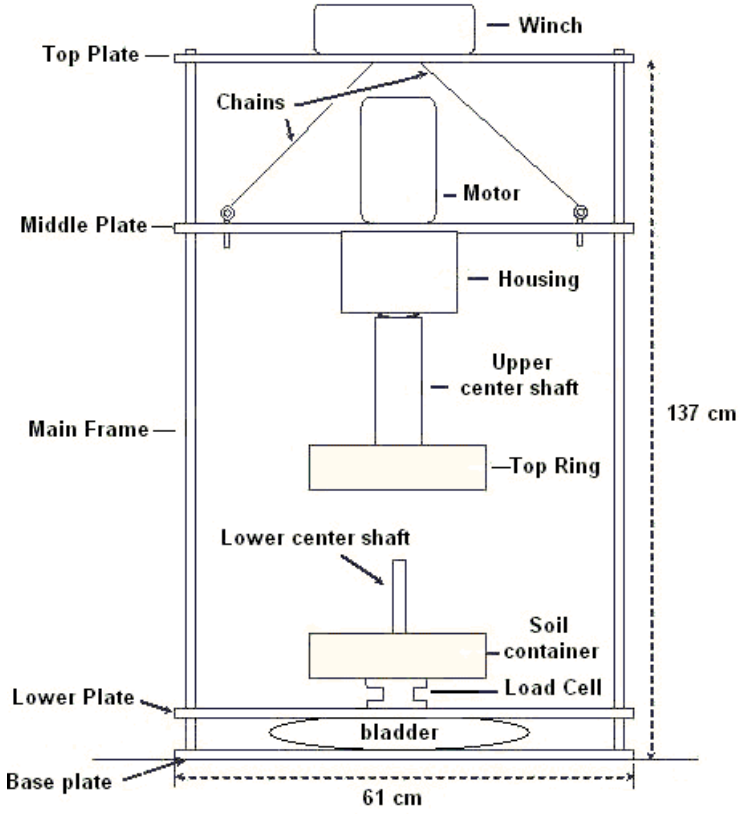


*Fig. 6. Schematic of Ring Shear Device*

top ring and the soil container is assured by a center shaft which fits into a set of low-friction linear bearings in the upper center shaft housing. The vertical confining stress on the sample is provided by first lowering the top ring assembly into contact with the sample and bolting the ring assembly to the base plate using vertical shafts attached to the middle plate. The top ring is thus prevented from moving vertically, and the contact pressure of the sand sample against the top ring can

then be controlled by applying regulated air pressure to a pneumatic bladder under the lower plate (Fig. 6). Horizontal cyclic and monotonic shear motion of the top plate can then be produced by the computer-controlled brushless servomotor.

Figure 7 is a schematic section of the hard-anodized aluminum sample container. The rotating top ring is sealed against the walls of the sample container by inner and outer o-rings. Walls of the container are smooth, but the container base and the top ring contact surface are roughened to insure coupling of shear stresses between the container and the sample. A layer of the test sand is epoxied to the container base, and the bottom surface of the top ring has a layer of aluminum oxide 40-grit wet-or-dry sandpaper glued to it. It was found to be easier to periodically replace this sandpaper after testing than to use an epoxied sand layer for the upper ring. No. 40 grit consists of 425 μm particles, but these do not entirely protrude from the sandpaper matrix, so the roughness is comparable to that of the test sand ($D_{50}$= 300 μm). Figure 7 also shows the trapezoidal cross-section of the sample container, with a base inclination $\alpha = 12^o$ intended to insure a uniform distribution

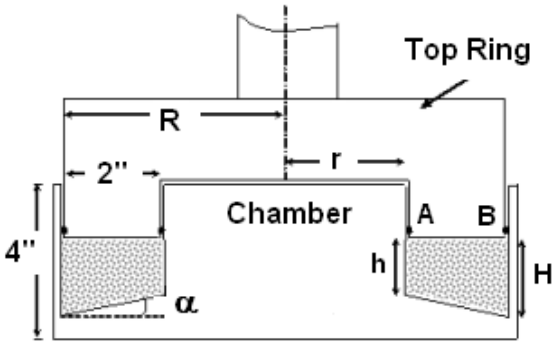


*Fig. 7. Cross- section of sample container. Base inclination $\alpha = 12^o$. R = 15.2 cm (6"), r = 10.2 cm (4").*

of horizontal shear strain across the specimen, as proposed by Yoshimi and Oh-Oka (1973).

Specimens were prepared by pluviation through a ring-shaped grid rainer. The rainer was first placed at the bottom of the chamber and filled with the required amount of sand; it was then pulled up through the sand fill to form the specimen. The top of the specimen was then leveled with a thin metal blade attached to a vacuum system, which removed excess material. Relative densities ranging from about 20% to 40% could be produced by varying the speed at which the rainer was withdrawn. Specimen uniformity was checked by dividing a test specimen into sections after gelatin impregnation (Garga and Sedano, 2002; Bennetts, 2003). A standard deviation of slightly over 1% in relative density was found between different sections.

All tests reported here were carried out with an initial vertical effective stress, $\sigma'_{vo}$ = 103.5 kPa (15 psi). Specimen saturation was achieved by circulating $CO_2$ and de-aired water through the specimen after slightly tilting the assembled loading frame, and then applying a back pressure of 103.5 kPa . A saturation index equivalent to the Skempton B-value was developed for this test chamber configuration, which indicated an initial degree of saturation in excess of 99.8% for all tests reported. All specimens were first liquefied under cyclic load (pore pressure ratio, $r_u$ =100%) and then subjected to monotonic load at top ring rotation speeds varying from 5 to 20 rpm, equivalent to average rotation velocities of 6.7 to 27 cm/sec. Ten revolutions were done at each rotation speed; resistance was observed to stabilize after about five full revolutions.

Figure 8 shows the results of a representative test at Dr = 27% Prior to each test, the empty chamber was assembled, filled with water and rotated at the speeds of the actual test to measure the o-ring friction values. These values were found to be on the order of 50% of the total 'raw' torque measure in the

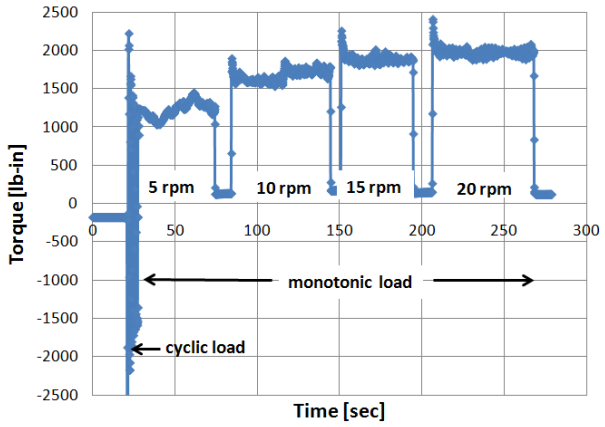


*Fig. 8. Test results for ring shear test at 27% relative density(1 lb-in = 0.113 Newton-meter)*

test. Residual shear (Sur) values calculated from the ring shear results of Fig.7, after correction for o-ring friction, are shown in Figure 9.

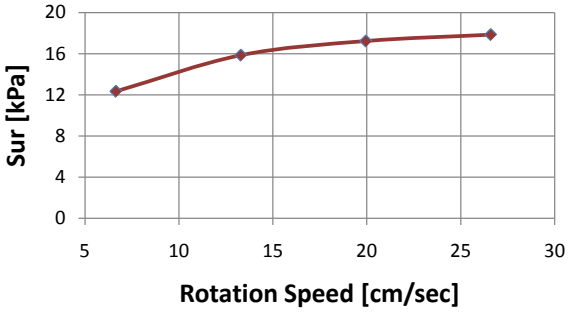


*Fig. 9. Residual strength (Sur) development at rotation speeds equivalent to 5, 10, 15, and 20 rpm, Dr = 27%*

We should also note that, as part of the calibration process, a special liquefaction test was carried out in which two diametrically- opposed columns of colored sand were formed

as the specimen was pluviated; results of this special test indicated that the thickness of the shear band in contact with the rotating ring was approximately 6 mm (0.24 in.), equivalent to 20 times $D_{50}$. This shear band thickness was used to compute the shear strains and shear strain rates reported below. The observed shear band thickness is greater than the 9 $D_{50}$ thickness reported for ring shear tests in sands of similar $D_{50}$ by Yoshimi and Kishida (1981); however the displacements reported in the latter study are only on the order of 1.2 cm, whereas the final cumulative displacement in our tests was about 3200 cm; it is possible to hypothesize that the thickness of the shear band evolves with accumulated displacement, as observed by Wafid et al. (2004) in split-ring shear tests on a non-plastic silt.

## DISCUSSION

Figure 10 (below) summarizes the results of successful ring shear tests on Holliston 00 sand, plotted against shear strain rate calculated from the shear band thickness described above. The behavior of the liquefied sand was that of a 'stress-thinning' material, in which shearing resistance increased, but at a decreasing rate, with shear strain rate. We concluded that the Herschel-Bulkley model best represented the observed behavior:

$$\tau = \tau_o + K \dot{\gamma}^{m} \qquad (1)$$

Where:

$\tau$: Shear stress, **K, m**: empirical parameters;

$\dot{\gamma}$ : Shear-strain rate, $\tau_o$ : 'yield shear stress' at $\dot{\gamma} = 0$

A Monte Carlo analysis was used to project the experimental curves back to the zero-strain-rate intercept ($\tau_o$) . Figure 11 summarizes the $\tau_o$ –values obtained from the analysis, and Fig. 12 the corresponding values of K and m. These results show that at densities over perhaps 50%, the $\tau_o$ –term controls Sur for this sand, and the contribution from increasing shear-strain rate becomes relatively small. This trend is already suggested by the curve for Dr = 36% in Fig. 10.

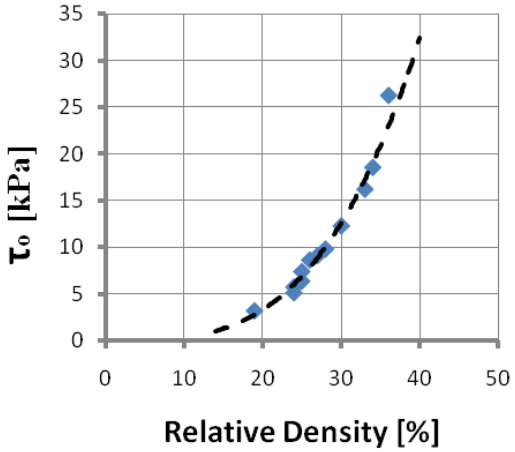


*Fig. 11. Variation of extrapolated ( $\tau_o$) values with relative density for Herschel-Bulkley Model*

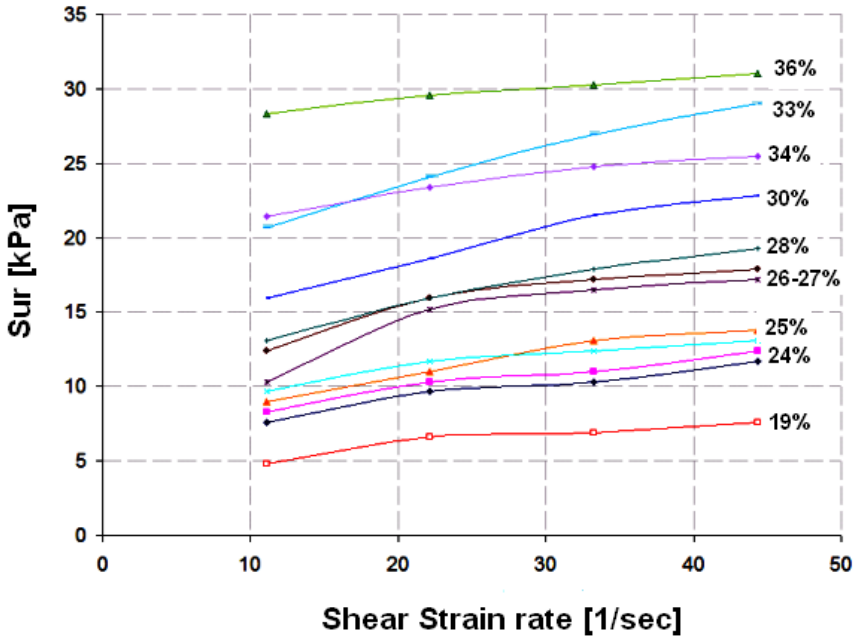


*Fig. 10. Summary of residual strength (Sur) values from ring shear tests. Relative density (Dr) values shown for each curve.*

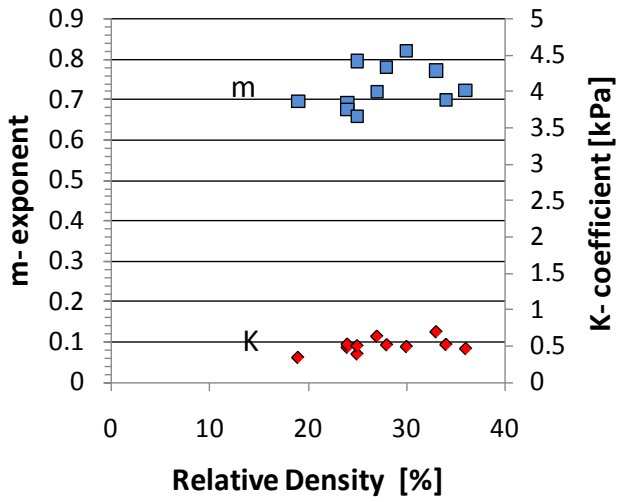


*Fig. 12. ( **K** ) and (**m**) parameters for Herschel-Bulkley model*

COMPARISON WITH FIELD VALUES

H. B. Seed (1987) proposed relating back-calculated Sur values from slope failures due to liquefaction with normalized field penetration resistance $(N_1)_{60}$ values from SPT tests, corrected for fines content to obtain equivalent clean sand values, $(N_1)_{60\text{-}cs}$. In 2007, Idriss and Boulanger published a critical review of available case histories, in which they listed those Sur-values they felt were best documented.

Figure 13 (next page) summarizes these results. This figure also compares these Sur-values with those obtained from the triaxial coupon and ring shear tests. In order to make this comparison, it was necessary to roughly convert lab test densities to standard penetration test (SPT) values. The most reasonable SPT values were found to be obtained using the lower-bound values of the conversion suggested by Cubrinovski and Ishihara (1999):

$$N_1 = C_d\,(Dr)^2 \qquad (2)$$

in which Dr is a ratio, not a percentage, and $C_d$ values depend on the difference in index void ratios, $e_{max}$ and $e_{min}$. A value of $C_d = 46$ was selected for this clean sand. Since these values were obtained for an energy ratio of 78%, a further normalization was required to obtain $N_1)_{60}$. It is interesting to note that the values obtained are practically the same as those that would be obtained using Mayne's (2001) relationship:

$$(N_1)_{60\text{-}CS} = 60 \cdot (Dr/100)^2 \qquad (3)$$

Shown in Fig. 13 are Sur-values obtained from the stabilized drag values of rough and smooth coupon tests. Ring shear test results displayed are for zero shear strain rate ($\tau_o$) and for a shear strain rate of 44 $sec^{-1}$, thus covering the range of values measured in these tests.

Also shown in the figure is a widely-used design curve relating median SPT-values to Sur, as presented by Idriss and Boulanger (2007). The figure clearly shows that rough and smooth coupon values follow the trend of the design curve, while the ring shear test Sur-values form an upper limit to the field cases.

This difference may reasonably be attributed to the difference in shear band behavior between the different tests. Arguably, a shear band forms around both coupons as they displace through the liquefied sand. It is reasonable to assume that he shear band thickness is controlled by the roughness of the contact surface, with the rough coupon forming the thicker band, but, very importantly, in both cases the sand in the shear band is free to dilate and thus produce a looser structure, whereas in the ring shear device no upward displacement of the top ring was detected, suggested that dilation was inhibited.

In this regard, it is worth noting that all the tests reported here are on the 'dry' side of critical, as indicated by their relative state parameter. (Boulanger, 2003) defined this parameter as:

$$\xi_R = 1/[Q - Ln\,(100p'/P_a)] - D_R \qquad (4)$$

This is a semi-empirical index which permits an approximation of the position of a given specimen relative to the critical state line. The first right-hand term represents the relative density at the critical state for the initial mean effective normal stress p'(normalized by atmospheric pressure $P_a$) , and Q is an empirical constant which determines the value of p 'at which dilatancy is suppressed; a Q value of 10 was used for this quartz sand.

Values obtained from equation (1) represent the position of the specimen relative to the critical state; $\xi_R < 0$ values indicate specimens on the 'dry' side of critical, and $\xi_R > 0$ values indicate material on the 'wet' side. In this context, all tests reported here have an initial $\xi_R < 0$, and thus would be considered dilative, although close to the critical state condition.

Consequently, these results suggest that the actual value of Sur in a specific case will depend very strongly on the geometry of the slope, and the particular boundary conditions of the shear band forming at the failure surface, with a shear band forming in the interior of a reasonably uniform liquefying mass representing a lower bound.

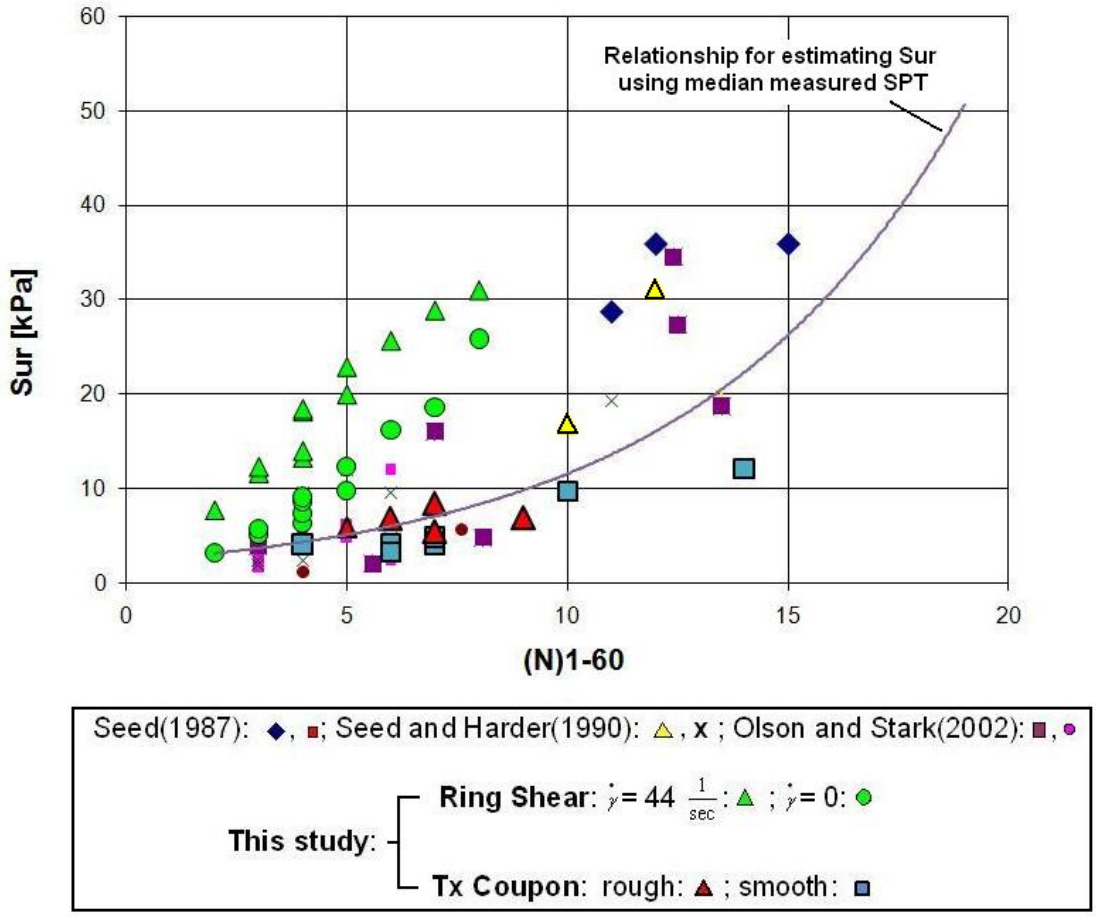


*Fig 13. Comparison of field Sur-values from Idriss and Boulanger (2007) with triaxial coupon and ring shear values*

ACKNOWLDGEMENTS

Construction of the triaxial device was funded by a Small Grant for Exploratory Research from the National Science Foundation. The ring shear project was supported by National Science Foundation Grant 0408945, and the device itself was built by a team of undergraduate Mechanical Engineering students at the University of New Hampshire: David Flynn, Robert Bouffard and Ruben Lingsay, as a senior capstone project under the direction of the authors. This material assistance and support is gratefully acknowledged.

REFERENCES

Bennetts, B. A. [2003], *" Effect of Specimen Preparation Technique on the Steady State Strength of Sands in the Ring Simple Shear Device,"* MS Thesis, Dept. of Civil and Environmental Engineering, University of Washington, Seattle.

Boulanger R., [2003], *"Relating $K_\alpha$ to relative state parameter index."* Journal of Geotechnical and Geoenvironmental Engineering, Vol. 129, No. 8, pp. 770-773.

Bryant, S., J. M. Duncan and H. B. Seed, [1983], *"Application of Tailing Flows Analyses to Field Conditions"*, Report UCB/GT/83-03 to US Bureau of Mines, Department of Civil Engineering, University of California, Berkeley, 312 pp.

Cubrinovski, M and Ishihara, I. (1999) *"Empirical correlation between SPT N-value and relative density for sandy soils."* Soils and Foundations, Vol. 39 No. 5, pp 61-71

de Alba, P. and T. P. Ballestero, [2006], *" Residual Strength after Liquefaction: A Rheological Approach,"* Soil Dynamics and Earthquake Engineering, Vol. 26, Nos. 2-4, February/April 2006, pp. 143-152**.**

de Alba, P. and T. P. Ballestero, [2008], *"Effect of Fines on Residual Strength after Liquefaction,"* Geotechnical Earthquake Engineering and Soil Dynamics IV, ASCE Geotechnical Special Publication 181.

Garga, V. K. and J. I. Sedano, [ 2002], *"Steady State Strength of Sands in a Constant Volume Ring Shear Apparatus,"* Geotechnical Testing Journal, Vol. 25 No. 4, pp.1-8.

Idriss, I. M., and R. W. Boulanger, [2007], *"SPT- and CPT-based Relationships for the Residual Strength of Liquefied Soils,"* 4th International Conference on Earthquake Geotechnical Engineering- Invited Lectures, pp. 1-22.

Mayne, P., B. Christopher and J. DeJong, [2001]. *"Manual on Subsurface Investigations,"* National Highway Institute, FHWA NHI-01-031.

Olson, S. M. and T. D. Stark, [2002], *"Liquefied Strength Ratio From Liquefaction Flow Failure Case Histories,"* Canadian Geotechnical Journal, Vol. 39, pp. 629-647.

Seed, H. B., [1987], *" Design Problems in Soil Liquefaction,"* Journal of the Geotechnical Engineering Division, ASCE, Vol. 113, No. 8, pp. 827-845.

Seed, R. and L. Harder, [1990], *"SPT-Based Analysis of Cyclic Pore Pressure Generation and Undrained Residual Strength,"* Proc. H. Bolton Seed Memorial Symposium, Vol. 2, pp. 351-376, BiTech Publishers Ltd.

Wafid Agung, M., K. Sassa, H. Fukuoka and G. Wang [2004], *"Evolution of Shear-Zone Structure in Undrained Ring-Shear Tests,"* Landslides, Vol.2, No. 1, pp 101-112.

Yoshimi, Y. and H. Oh-Oka, [1973], *"A Ring Torsion Apparatus for Simple Shear Tests,"* Proc. 8th International Conference on Soil Mechanics and Foundation Engineering, Moscow, Russia, pp. 501-506.

Yoshimi, Y. and T. Kishida, [1981], *"A Ring Torsion Apparatus for Evaluating Friction Between Soil and Metal Surfaces,"* Geotechnical Testing Journal, Vol. 4, No. 4, pp 145-152.